FORMATION OF A CHARGED LAYER IN A BOUNDED NON-UNIFORM MAGNETIZED PLASMA IN RF FIELD

V.I. ZASENKO

Bogolyubov Institute for Theoretical Physics, Nat. Acad. of Sci. of Ukraine
(14-b, Metrologichna Str., Kiev 03680, Ukraine; e-mail: zasenko@bitp.kiev.ua)

PACS 71.20.Nr; 72.20.Pa

A model of plasma dynamics in the box of an ICRF (ion cyclotron radio-frequency) antenna without Faraday shield used for the plasma heating in tokamaks is proposed. Formation of a macroscopic layer of oscillating charge that plays a role of a shield is predicted. Relation to phenomena observed in a scrape-off layer plasma is discussed.

1. Introduction

It is well known that one of the main properties of a plasma is its ability to redistribute charges so that the stationary external electric field is shielded. Thus, a calm bulk plasma remains quasineutral, meanwhile the shielding charge forms sheaths localized around boundary surfaces. The sheath potential balances ion and electron fluxes to boundaries so to keep the bulk plasma quasineutrality. We predict that a similar, however more complex, structure would appear in the box of an unshielded ICRF antenna used for the plasma heating in tokamaks. The structure is a macroscopic layer of oscillating charge, which is formed in a laterally bounded strongly non-uniform magnetized plasma under strong radio-frequency (RF) radiation. We consider the formation of a charge layer, as well as the shielding of the potential component of a RF field and other observable effects for a typical geometry and plasma parameters of unshielded ICRF antennas.

In present-day implementations in the ICRF antennas, electromagnetic radiation is launched into a plasma by arrays of antennas composed of current straps (termed central conductors) running poloidally in a tokamak and surrounded laterally by metallic walls, which form a protective antenna box (see Fig. 1). Since an early date, ICRF experiments have been conducted with a Faraday shield (FS) placed between the antenna and the plasma, FS currently in use being composed of an array of metallic blades placed over the mouth of the antenna box. FS gives the electromagnetic radiation with favorable polarization and isolates the central conductors from the edge plasma [1–3]. Positive effects of FS are nevertheless accompanied by adverse ones. These include the suppression of the magnetic flux of the central conductor [4] and the sputtering of heavy ion impurities from the shield surface due to the RF sheath effect [5–8].

After the re-evaluation of the role of FS [9], a number of experiments with unshielded antennas was fulfilled on different tokamaks [10–18]. Most of them showed the successful operation of an unshielded ICRF antenna, others gave a degradation of heating parameters.

These experiments have motivated the development of the model of plasma dynamics in an unshielded antenna box given in the present paper, preliminary results of which have been presented in references [19–21]. Plasma behavior in the electric *potential* field driven by a central conductor was self-consistently treated there. Later, the *inductive* poloidal component of an electric field was accounted in the extended model [22, 23]. The latter gave additional data on a distribution of poloidal components of an electric field and particle fluxes, but it showed at the same time that the effect of a poloidal field on particle densities in an antenna box is rather small. Here, to concentrate on the main effects in an antenna box, we do not treat the inductive component of a RF field self-consistently, but keep it in equations to discuss why its influence is small.

In this paper, the distributions of particle densities and the field along the box depth are examined, and their variations on the RF time scale and the secular

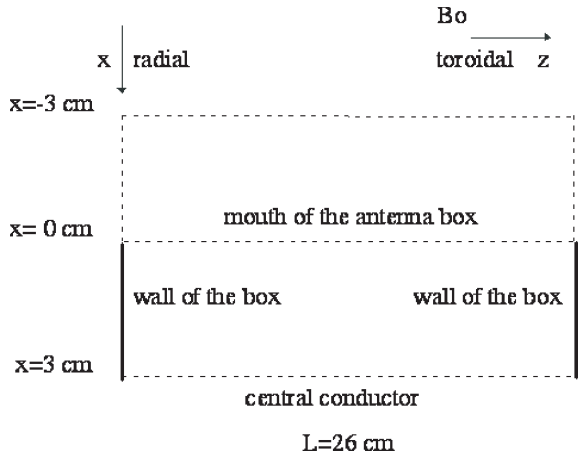

Fig. 1. Poloidal view of the antenna box with a toroidal extension of 26 cm and a radial extension of 3 cm. The plasma layer of thickness 3 cm in front of the box is also considered in the model. The central conductor is taken to be the surface at x=3 cm of width L=26 cm and to have a potential given by Eqs. (14), (15); the walls of the box are at potential $\bar{\varphi} = 0$

evolution for an interval of hundreds of RF periods are studied. The current flowing into the antenna box and the power dissipation caused by the particle acceleration in the drop of the potential between the plasma and the grounded box (i.e. in the sheath) are calculated. Phenomena observed in the scrape-off layer plasma during the ICRF antenna operation such as a plasma density profile modification, the generation of harmonics and a stationary field, current rectification, and sheared $\mathbf{E}\times\mathbf{B}$ poloidal flow are discussed.

Important issues for experiments include the evaluation of a density profile modification by the RF field, the power dissipation in sheaths, associated sputtering, and current rectification. The experimental evidence of sheath effects is reported in [24–26].

The focusing of the present work on very near-field, electrostatic effects distinguishes it, in spirit, from works [5–7], where the inductively driven electric field was envisaged. The ultimate modeling of this inductive field in electrostatic terms in these references did not treat the radial variations studied here. Interest in these variations is heightened by the absence of FS, which is another distinguishing feature of our work.

2. Model

2.1. Basic equations

Periodic potential ≈ 20 kV applied to the central conductor produces a strong electrostatic field, which is shielded in a space interval about 3 cm and is taken to dominate the inductive effects in this region. The plasma dynamics in the antenna box is determined by a balance between the particle transport in the radial direction across magnetic lines and the particle escape to the box walls along magnetic lines (Fig. 1).

It is known that the edge plasma is characterized by a high level of turbulence which causes the anomalous transverse diffusion. In stationary situations such as a probe in a magnetic field [27–31] and the density and potential profiles of a scrape-off layer plasma [32–34], the cross-field diffusion is often considered without specification of a detailed mechanism. The transverse motion is described by diffusion-type equations with anomalous transport coefficients. To justify the diffusion approximation in the present non-stationary problem with RF field, we start from the two-fluid MHD and Poisson equations. Assuming the poloidal (y) invariance, these equations read

$$\frac{\partial}{\partial t}n_\alpha + \frac{\partial}{\partial x}\left(n_\alpha V_{\alpha x}\right) + \frac{\partial}{\partial z}\left(n_\alpha V_{\alpha z}\right) = 0, \tag{1}$$

$$m_\alpha n_\alpha \left\{\frac{\partial}{\partial t} + V_{\alpha x}\frac{\partial}{\partial x} + V_{\alpha z}\frac{\partial}{\partial z}\right\} V_{\alpha x} =$$

$$= q_\alpha n_\alpha \left(E_x + V_{\alpha y}B_0/c\right) - T_\alpha \frac{\partial n_\alpha}{\partial x} - \nu_{\perp\alpha} m_\alpha n_\alpha V_{\alpha x}, \tag{2}$$

$$m_\alpha n_\alpha \left\{\frac{\partial}{\partial t} + V_{\alpha x}\frac{\partial}{\partial x} + V_{\alpha z}\frac{\partial}{\partial z}\right\} V_{\alpha y} =$$

$$= q_\alpha n_\alpha \left(E_y - V_{\alpha x}B_0/c\right) - \nu_{\perp\alpha} m_\alpha n_\alpha V_{\alpha y}, \tag{3}$$

$$m_\alpha n_\alpha \left\{\frac{\partial}{\partial t} + V_{\alpha x}\frac{\partial}{\partial x} + V_{\alpha z}\frac{\partial}{\partial z}\right\} V_{\alpha z} =$$

$$= q_\alpha n_\alpha E_z - T_\alpha \frac{\partial n_\alpha}{\partial z}, \tag{4}$$

$$\left(\frac{\partial^2}{\partial x^2} + \frac{\partial^2}{\partial z^2}\right)\varphi = 4\pi e\left(n_e - n_i\right). \tag{5}$$

Here, n_α is the particle density, $\mathbf{V}_\alpha$ – fluid velocity, m_α and q_α – particle mass and charge, T_α – temperature, α – species index, E_x, E_z – components of the potential field characterized by potential φ, E_y – poloidal component of the inductive field. For simplicity, we assume only one ion species in Eq. (3) with $q_i = e$.

The effective collision frequency $\nu_{\perp\alpha}$ describes a change in the particle momentum due to collisions with a turbulent field. The magnitude of anomalous diffusion coefficient observed in experiments, $D \approx 4$ m^2/s, corresponds to each effective collision frequency, being of the order of the cyclotron frequency for its species, $\omega_{c\alpha}$; that is, of the order of or higher than the frequency of the driving field. In view of this, the inertial terms in Eqs. (2) and (3) are neglected, yielding the transverse diffusion equations for particle densities in the RF case.

The system under consideration is strongly varying in the radial direction, but quite uniform along the magnetic field lines due to the difference in transverse and longitudinal box dimensions. Thus, the parallel invariance holds to a fair degree in the rarefied plasma region nearest to the central conductor. In the domain where plasma is dense enough to form a thin sheath layer between the box wall and the bulk plasma, the uniformity along magnetic lines in the bulk (i.e. outside the sheath) region becomes even higher. This uniformity of the particle densities and the potential in the bulk region allows us to introduce variables averaged over the box width according to

$$\bar{n} = \frac{1}{L} \int\limits_{-L/2}^{L/2} n dz. \tag{6}$$

With neglect of inertial terms, the equations for the averaged densities and the potential following from Eqs. (1)–(3) and (5) take the form

$$\frac{\partial \bar{n}_\alpha}{\partial t} - \frac{\partial}{\partial x} D_{\alpha x} \left[\frac{\partial \bar{n}_\alpha}{\partial x} + \bar{n}_\alpha \frac{q_\alpha}{T_\alpha} \left(\frac{\partial \bar{\varphi}}{\partial x} - \frac{\omega_{c\alpha} \bar{E}_y}{\nu_{\perp\alpha}} \right) \right] +$$

$$+ \frac{2}{L} \left[n V_z \right]_\alpha = 0, \tag{7}$$

$$\frac{\partial^2 \bar{\varphi}}{\partial x^2} = 4\pi e \left(\bar{n}_e - \bar{n}_i \right), \tag{8}$$

where

$$D_\alpha = \frac{T_\alpha}{m_\alpha} \frac{\nu_{\perp\alpha}}{\nu_{\perp\alpha}^2 + \omega_{c\alpha}^2},$$

and $\nu_{\perp\alpha}$ are chosen to yield $D_\alpha = 4$ m^2/s. To close the system of equations (6), (7), the fluxes to the walls at $z = \pm L/2$, $[nV_z]_\alpha$, should be written in terms of $\bar{n}$ and $\bar{\varphi}$.

2.2. Particle fluxes to the wall

I. Quasineutral plasma. The potential in the bulk quasineutral plasma varies in the transverse x-direction and remains flat in z along the magnetic lines. Almost all the potential drop along magnetic lines between the plasma and the grounded antenna box ($\varphi = 0$) occurs in a near vicinity of the wall of the antenna box, namely in the sheath. The sheath is formed on the time scale given by the inverse electron plasma frequency, i.e. much faster than on the RF scale. In accordance with the probe theory [27–30] and studies of the RF sheath [7,35], we assume that, in the absence of a substantial accelerating field in the bulk region, particles enter the sheath with velocities of the order of the thermal one, $V_{Te} = (T_e/m_e)^{1/2}$, for electrons and of the sound speed, $c_s = ((T_e + \gamma T_i)/m_i)^{1/2}$, for ions with $\gamma = 2$ [11]. The particle density, which determines the flux, is considered to be the averaged density $\bar{n}_\alpha$. When the potential difference between the bulk plasma and the wall (i.e. across the sheath) is retarding, the flux is reduced in the sheath by the Boltzmann factor, which corresponds to the neglect of inertial terms in Eq. (4). This gives the particle fluxes to the wall in the form

$$[nV_z]_i = \begin{cases} \bar{n}_i c_S & (\bar{\varphi} > 0), \\ \bar{n}_i c_S \exp(e\bar{\varphi}/T_i) & (\bar{\varphi} < 0), \end{cases} \tag{9}$$

$$[nV_z]_e = \begin{cases} \bar{n}_e V_{Te}/\sqrt{2\pi} & (\bar{\varphi} < 0), \\ \bar{n}_e V_{Te}/\sqrt{2\pi} \exp(-e\bar{\varphi}/T_e) & (\bar{\varphi} > 0). \end{cases} \tag{10}$$

II. Non-quasineutral plasma. In the 1D case, the requirement of constant potential along the magnetic lines (zero electric field) corresponds to the condition of plasma quasineutrality. In the 2D case with radial (x) variation, this requirement does not imply quasineutrality; for example, in the slab (capacitor) geometry, an infinite sheet distribution of charge with limited transverse extent and uniform one along magnetic lines produces a variation of the potential only in the transverse direction. We further distinguish two cases relevant to the present 2D case of a distribution under a relatively limited transverse x-dimension, which is additionally finite in the z-direction: *a)* the total charge density at some fixed radial position is of opposite sign relative to the charge on the antenna (termed a "normal" population of particles) and *b)* the charge has the same sign (termed an "inverted" population of particles).

IIa. Non-quasineutral plasma, normal population of particles. In the case where the population of particles at some given layer is normal, the central conductor of the

antenna constitutes one plate of the capacitor, and the layer represents the other "plate" with opposite charge. The electric field tends to have only a radial component (outside a restricted fringing region at the "capacitor" edges), the more as the opposed charge magnitudes become equal. Therefore, we approximate the field component along the magnetic lines as zero everywhere outside the sheath. The same considerations as employed for a 1D quasineutral plasma can then be applied to this case with particle fluxes taken in the form (9), (10).

IIb. Non-quasineutral plasma, inverted population of particles. If the population of particles is inverted at some given layer, this layer constitutes the other "plate" of a capacitor with the same sign of charge as that on the central conductor. The electric field topology is changed, and the field directed along the magnetic lines penetrates into the plasma further than the sheath thickness, unlike the two previous cases *I, IIa.* This causes a higher rate of particle expulsion along the magnetic lines to the walls until the population in the layer becomes normal, whereupon the flow proceeds in accordance with the previous case. The enhanced fluxing from the layer with inverted population takes place on a time scale shorter than the RF period. This enhanced flux is heuristically modeled as the averaged density times the velocity of free fall out of the plasma at potential $\bar{\varphi}$

$$[nV_z]_\alpha = \bar{n}_\alpha \sqrt{2e\bar{\varphi}/m_\alpha}. \tag{11}$$

Summarizing in a form including Eqs. (9) and (10), we take the particle fluxes to the walls as follows:

$$[nV_z]_i = \begin{cases} \bar{n}_i c_S + \bar{n}_i \sqrt{2e\bar{\varphi}/m_i}\ \vartheta(1-\bar{n}_e/\bar{n}_i) & \\ \qquad\qquad (\bar{n}_i > \bar{n}_e, \bar{\varphi} > 0), & \\ \bar{n}_i c_S \qquad\qquad (\bar{n}_i < \bar{n}_e, \bar{\varphi} > 0), & \\ \bar{n}_i c_S \exp(e\bar{\varphi}/T_i) \qquad\qquad (\bar{\varphi} < 0), & \end{cases} \tag{12}$$

$$[nV_z]_e = \begin{cases} \bar{n}_e V_{Te}/\sqrt{2\pi} + & \\ +\bar{n}_e \sqrt{-2e\bar{\varphi}/m_e}\ \vartheta(1-\bar{n}_i/\bar{n}_e) & \\ \qquad\qquad (\bar{n}_i < \bar{n}_e, \bar{\varphi} < 0), & \\ \bar{n}_e V_{Te}/\sqrt{2\pi} \qquad (\bar{n}_i > \bar{n}_e, \bar{\varphi} < 0), & \\ \bar{n}_e V_{Te}/\sqrt{2\pi} \exp(-e\bar{\varphi}/T_e) \qquad (\bar{\varphi} > 0). & \end{cases} \tag{13}$$

In Eqs. (12) and (13) the function $\vartheta((1-\bar{n}_\alpha/\bar{n}_\beta))$, with properties $\vartheta(0) = 0$ (normal population) and $\vartheta(1) = 1$ (inverted population), is introduced as a factor. Being a rounded step function, it smoothens the transition in the flux terms between the cases of normal and inverted populations. The enhanced flux terms in Eqs. (12) and (13) play a crucial role in the general behavior of a particle density in the box. When, at some radial position and at some instant, a layer has an inverted population of particles, the additional flux causes fast – on the scale of the RF period – return of the system to a state with the normal population of particles. With the neglect of such an expulsion, a non-neutralized tail on the decreasing spatial distribution of ion density can persist in the region of rare plasma nearest to the central conductor. The evolution of the system is sensitive to the presence of this non-physical tail.

2.3. Boundary conditions at the central conductor and in front of the box

The boundary conditions for the potential and particle densities at the position of the central conductor, $x = d(= 3$ cm), are straightforward

$$\bar{\varphi}(d) = \varphi_0 \sin(2\pi f t) \quad \text{for RF excitation,} \tag{14}$$

and

$$\bar{\varphi}(d) = \varphi_{\text{fl}} \quad \text{in the stationary state without RF,} \tag{15}$$

where the floating potential

$$\varphi_{\text{fl}} = (T_e/e)\ \ln(v_{Te}/c_S\sqrt{2\pi}).$$

We suppose that there is no plasma at this position

$$\bar{n}_i(d) = \bar{n}_e(d) = 0. \tag{16}$$

The boundary conditions for particle densities may be taken in another form than the homogeneous one without a significant influence of the results.

To avoid an arbitrary specification of the boundary condition at the box mouth, $x = 0$, we also consider the plasma dynamics in front of the box. The same equations (7) and (8) are applied over the same region in z as inside the box, but with modified fluxes along the magnetic lines:

$$[nV_z]_i = \begin{cases} \bar{n}_i c_S \left[1 - \exp\left(-\dfrac{e(\bar{\varphi}-\varphi_{\text{fl}})}{T_i}\right)\right] & \\ \qquad\qquad (\bar{\varphi} > \varphi_{\text{fl}}), & \\ \bar{n}_i c_S \left[-1 + \exp\left(\dfrac{e(\bar{\varphi}-\varphi_{\text{fl}})}{T_i}\right)\right] & \\ \qquad\qquad (\bar{\varphi} < \varphi_{\text{fl}}), & \end{cases} \tag{17}$$

$$[nV_z]_e = \begin{cases} \dfrac{\bar{n}_e V_{Te}}{\sqrt{2\pi}} \left[-1 + \exp\left(-\dfrac{e(\bar{\varphi} - \varphi_{\text{fl}})}{T_e} \right) \right] \\ \qquad\qquad (\bar{\varphi} > \varphi_{\text{fl}}), \\ \dfrac{\bar{n}_e V_{Te}}{\sqrt{2\pi}} \left[1 - \exp\left(\dfrac{e(\bar{\varphi} - \varphi_{\text{fl}})}{T_e} \right) \right] \\ \qquad\qquad (\bar{\varphi} < \varphi_{\text{fl}}). \end{cases} \quad (18)$$

These relations describe the fluxes of charged particles in front of the box through imaginary surfaces at $z = \pm L/2$ in reaction to the z-variation of the potential, which remains after the shielding by the plasma in the antenna box. The first terms represent free-streaming effluxes from the region with higher potential energy of particles, and the second are particle influxes to the same region suitably reduced by the Boltzmann factor, where the potential is taken as φ_{fl} at large $|z|$ (corresponding to the scrape-off plasma making contact with a grounded $\varphi = 0$ tokamak limiter). Due to the free flow of particles from the region toroidally beyond the box sides, the potential in front of the box is shielded more effectively than that in the presence of box walls (at a small distance $\Delta x \approx 1$ mm). Consequently, the particle density and potential profiles are rather insensitive to the boundary condition imposed on the potential at $x = -d$ ($= -3$ cm), the first of the following conditions:

$$\begin{aligned} &\frac{\partial \bar{\varphi}}{\partial x}(-d) = k\left(\bar{\varphi}(-d) - \varphi_{\text{fl}}\right), \\ &\bar{n}_i(-d) = n_0, \\ &\bar{n}_e(-d) = n_0. \end{aligned} \quad (19)$$

The first condition states that the potential decays in the plasma to the floating value with characteristic length k^{-1}. At the box mouth interface, $x = 0$, the particle densities and fluxes, potential, and radial electric field are continuous:

$$\bar{n}_\alpha(+0) = \bar{n}_\alpha(-0),$$

$$\left[\frac{\partial \bar{n}_\alpha}{\partial x} + \bar{n}_\alpha \frac{q_\alpha}{T_\alpha} \left(\frac{\partial \bar{\varphi}}{\partial x} - \frac{\omega_{c\alpha} \bar{E}_y}{\nu_{\perp\alpha}} \right) \right]_{+0} =$$

$$= \left[\frac{\partial \bar{n}_\alpha}{\partial x} + \bar{n}_\alpha \frac{q_\alpha}{T_\alpha} \left(\frac{\partial \bar{\varphi}}{\partial x} - \frac{\omega_{c\alpha} \bar{E}_y}{\nu_{\perp\alpha}} \right) \right]_{-0},$$

$$\bar{\varphi}(+0) = \bar{\varphi}(-0),$$

$$\frac{\partial \bar{\varphi}}{\partial x}(+0) = \frac{\partial \bar{\varphi}}{\partial x}(-0). \quad (20)$$

Thus, the model describes two plasmas, inside the antenna box and in front of the box, which are governed by the same system of equations (7), (8), but with different fluxes along the magnetic lines. Equations (12) and (13) give the fluxes for plasma particles to the walls inside the box. These fluxes are subdivided into the normal ($\vartheta = 0$) and inverted ($\vartheta = 1$) cases, the former coinciding with the result of the probe theory, and the latter reflecting an increased flux due to the enhanced penetration of the electric field component parallel to the magnetic field. The inverted state evolves rapidly on the scale of the RF period. In this case, the excess particles with inverted population are expelled with a velocity faster than the thermal one until the inverted layer becomes normal. After this, the expulsion will continue, but with the thermal velocity. In front of the box at the toroidal position of the box wall, there is no solid boundary, and particle flow along the magnetic lines is free in both directions. Equations (17) and (18) describe the fluxes in front of the antenna box at this position. The equations describing the two plasmas are coupled through the boundary conditions (20) at the common interface $x = 0$. In addition, the solution for the plasma inside the box must satisfy the boundary conditions (14)–(16) at $x = d$ (central conductor), and that for the plasma outside the box at $x = -d$ satisfies the boundary conditions (19).

3. Particle Densities and Potential

The equations obtained in the previous section have been solved numerically, and the results are given below. Deuterium plasma parameters, taken in the numerical simulations, are as follows: 0.5×10^{18} m^{-3} $\leq \bar{n}_\alpha(x = -3 \text{ cm}) \leq 2 \times 10^{19}$ m^{-3}, $m_i = 2m_p$, $T_i = 60$ eV, $T_e = 30$ eV, $B_0 = 3T$, $f = 3 \times 10^7$ Hz, $\varphi_0 = 20$ kV, $D = 4$ m^2/s, $k = 12.1$ m^{-1}. The results presented in the figures relate to $\bar{n}_\alpha(x = -3 \text{ cm}) = n_0 = 2 \times 10^{18}$ m^{-3}. In the figures, the particle density is normalized to n_0 and $U = e\bar{\varphi}/T_e$ is the dimensionless potential. In the calculations, we omit the poloidal component of the inductive field E_y from Eqs. (7) and (20); the effect of E_y was considered in works [22, 23] and is discussed in Section 5.

3.1. Evolution in the early stage

The early stage of evolution of the particle density and the self-consistent potential from the stationary state without RF field is presented in Figs. 2–4 for the upper part of the box. The time interval extends over the first 45 periods after the RF potential is applied, f being

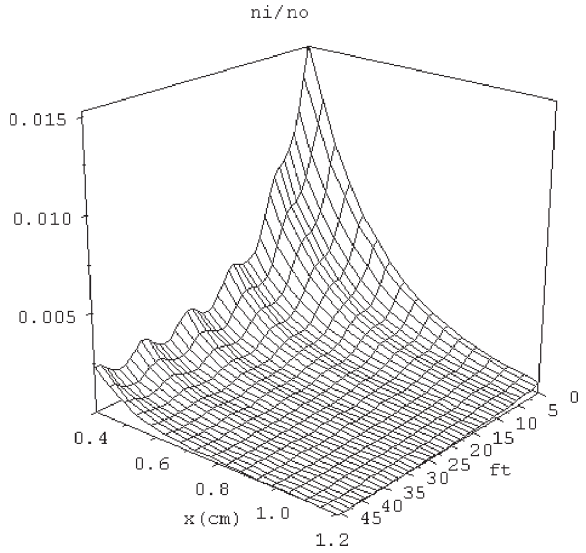

Fig. 2. Evolution of the ion density $\bar{n}_i/n_0$ over the first 45 periods after RF voltage is applied. The time interval between two lines is taken as 1.125 RF period f^{-1} to give the slower stroboscopic view of oscillations. The upper part of the antenna box is shown, for x between 0.4 and 1.2 cm (see Fig. 1)

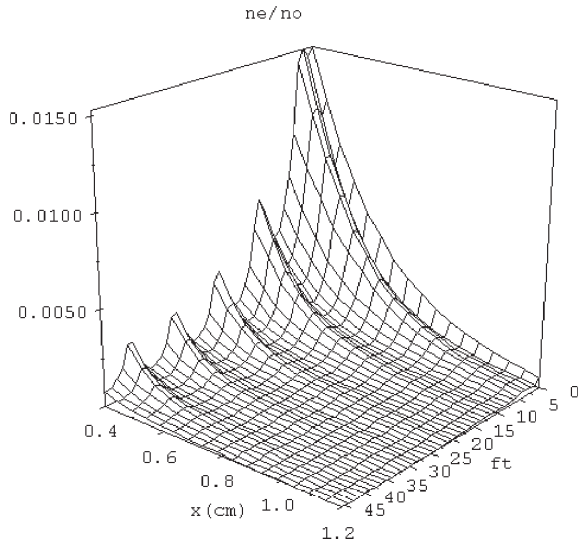

Fig. 3. Same as in Fig. 2, but showing the electron density in place of ion one. Electron expulsion proceeds with a larger oscillation than that of ions

the applied frequency. The greatly reduced number of oscillations is due to the stroboscopic sampling. Because of a larger mass, the ion expulsion from the density tail (Fig. 2) proceeds with moderate oscillations in the ion density, whereas the expulsion for electrons (Fig. 3) takes place with larger oscillations. A concurrent widening of the region with very rare plasma occurs, as was seen

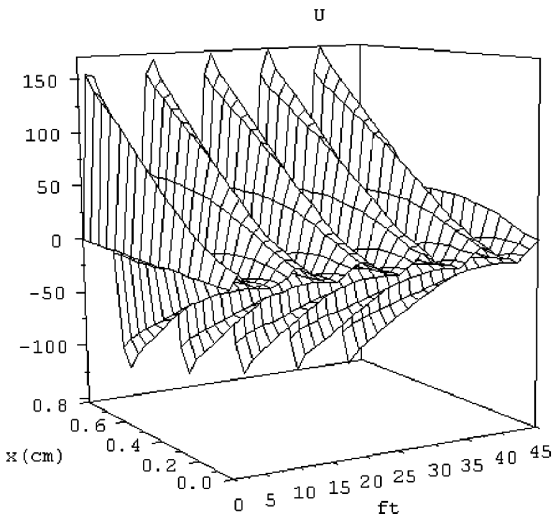

Fig. 4. Evolution of the potential $U = e\bar{\varphi}/T_e$ with same time interval and stroboscopic sampling as in Figs. 2 and 3. The upper part of the antenna box is shown, for x between 0 and 0.8 cm (see Fig. 1). The directions of both x and t axes are changed as compared with Figs. 2 and 3 for a better view. The penetration of the potential into the plasma corresponds to a relative depletion of the density tail

in experiment [36]. The evolution of the self-consistent potential is shown in Fig. 4 (in this figure, the direction of the x and t-axes has been switched for a better view). The penetration of the potential into the plasma proceeds simultaneously with the above expulsion of particles from the density tail. The potential in the dense plasma domain, where a sheath is formed at the wall, exhibits asymmetrically positive oscillations with respect to the dimensionless floating potential $U_{\text{fl}} = 2.381$; this will appear even more clearly in the case of converged steady-state oscillations (at $x = 0$ in Fig. 10). When the potential in the plasma gets below the floating value, this results in the intense flow of electrons out of the plasma with velocities typically of the order of the electron thermal velocity. The plasma becomes more positively charged, and its potential returns to a value close to the floating potential, such relaxation being rapid on the RF time scale. In the theory of a RF sheath, where the bulk plasma is quasineutral, this phenomenon leads to the RF sheath rectification effect [5–7, 37]; in the case under consideration, the plasma may lose its quasineutrality.

3.2. Layered structure

After several hundreds of RF periods, the evolution becomes very slow with changes in quantities over successive periods with the doubling of the time interval giving

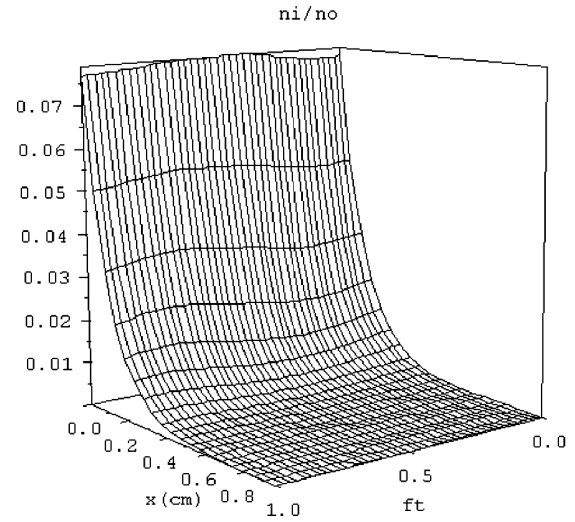

Fig. 5. Plasma (ion) density $\bar{n}_i/n_0$ over one period, 800 RF periods after the RF voltage was applied. The upper part of the box is shown, for x between 0 and 1 cm (see Fig. 1)

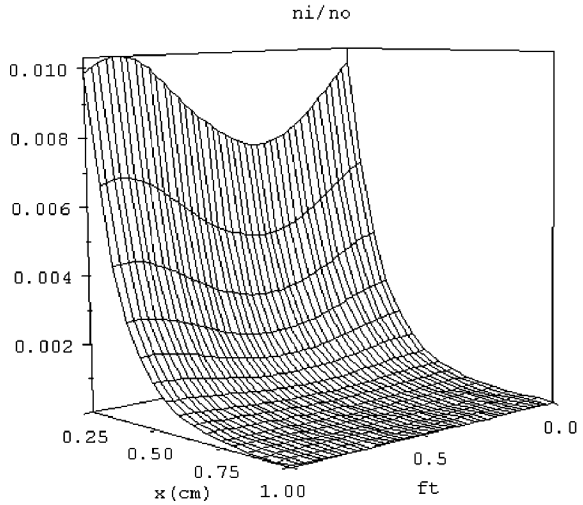

Fig. 6. Same ion density as in Fig. 5 but with higher resolution making the oscillations more visible

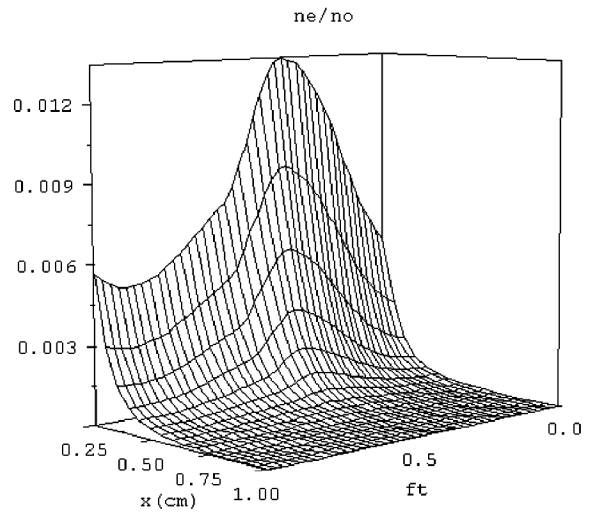

Fig. 7. Plotted oscillations in the electron density $\bar{n}_e/n_0$ have a larger amplitude than the corresponding ion oscillations (Fig. 6), and are in opposite phase

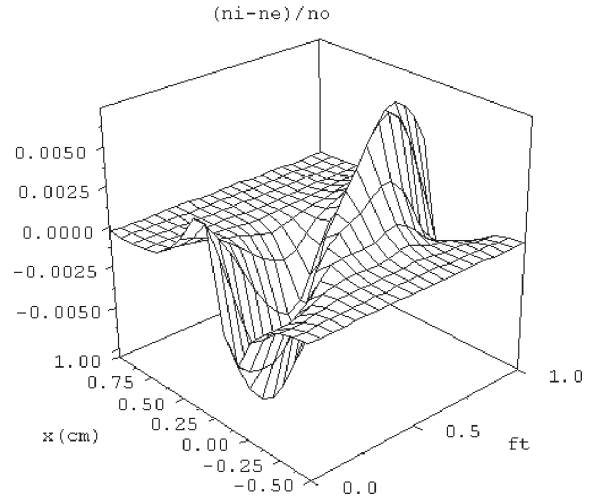

Fig. 8. Difference in the ion and electron densities, $(\bar{n}_i - \bar{n}_e)/n_0$, over one period, 800 RF periods after RF voltage was applied. Charge separation is localized to a layer with a thickness of several mm coinciding with the position, where the potential has a large radial second derivative

no visible change on the graphical output, by indicating the numerical convergence. At this stage, the plasma has been expelled from the region near the central conductor, as is shown in Fig. 5 (see also Fig. 12), this is effectively a vacuum region. There follows a region of steep increase in the density. If we consider the antenna central conductor as one plate of the capacitor, the region, where plasma begins to be dense, forms the other "plate" or charged layer, where the charge density varies strongly each half-period. Here, the main shielding of the antenna potential takes place. Oscillations of the ion and electron densities in this region, with higher resolution than in Fig. 5, are shown in Figs. 6 and 7. The densities oscillate in opposite phases, and the amplitude of electron density oscillations is higher than that of ions. (When the frequency of the driving potential increases, this asymmetry becomes more pronounced). Figure 8 shows that the charge separation (difference in the ion and electron densities) is localized to a region near the box mouth ($x = 0$). Further toward the exterior of the box, there follows the region of quasineutral plasma, beginning either inside or outside the box depending on

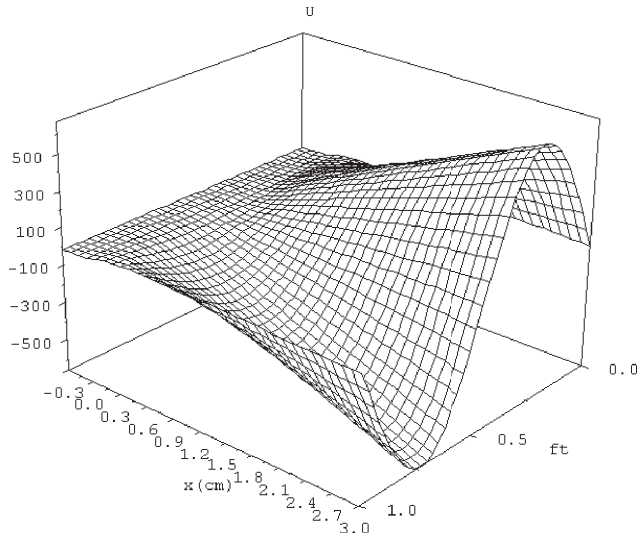

Fig. 9. Distribution of the scaled potential $U = e\bar{\varphi}/T_e$ over one period, 800 periods after the application of excitation (stationary regime). The flat region at negative x shows that the effective shielding takes place in a vicinity of the mouth of the box. High spatial second derivative corresponds to the domain of large charge separation (see Fig. 8)

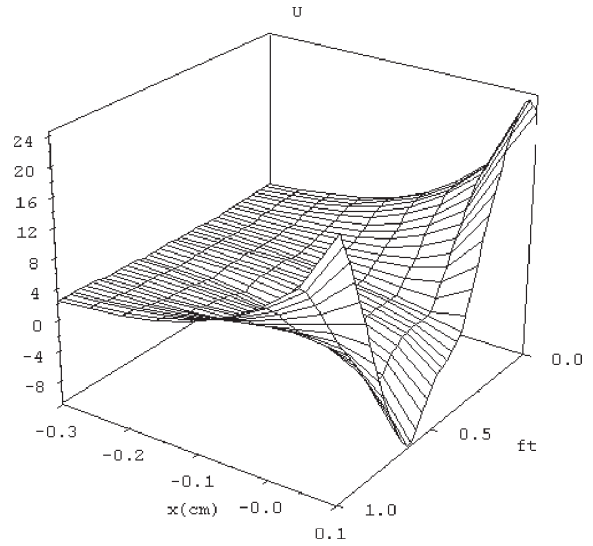

Fig. 10. Higher resolution plot of the potential of Fig. 9 showing the shielding to the floating value $U_{\rm fl} = 2.381$ at one or two millimeters in front of the box mouth

the density at the box mouth. The potential distribution (Fig. 9) reflects a variation of particle density profiles. In the vacuum region, the potential drop is linear, of course. There follows the region of a high radial second derivative corresponding to the high charge separation. Proceeding further into the quasineutral plasma, the potential flattens, i.e., the electric field is essentially shielded. Except for the vacuum region, the potential does not get substantially below the floating value, as was discussed in the previous section. Thus, we can distinguish three different regions in the antenna box. Since the plasma is strongly expelled to the walls, the region nearest to the central conductor is essentially a vacuum one with a linear radial variation of the potential; a considerable drop of the potential occurs along the magnetic lines in this vacuum region. Despite this fact, the sputtering is not dangerous, since the extremely low plasma density precludes a thin sheath being formed. Relatively few ions that are present cannot be accelerated across the broad potential drop in a half period. Near the mouth of the box, there is a second region of a comparatively dense plasma with high oscillating charge density, the charged layer. The rest of the potential drop over x occurs in this region, where the potential is shielded; still further out of the box, there is the third region, where the electric field is relatively weak. For a low density at the mouth of the box, $n_i < 0.5 \times 10^{18}$ m^{-3}, and the potential at the central conductor of 20 kV, the charged layer extends to the mouth of the box. If the plasma at the box mouth is appreciably more dense than this value, the bulk of the shielding is completed at some distance inside the box. The most intense sputtering due to the RF sheath effect can be expected around that radial position, where, on the one hand, the plasma density has become sufficiently high to form a thin sheath at the box wall, and, on the other hand, the potential is still large enough to maintain the sputtering.

4. Effects of a RF Potential Field on Plasma Near the Antenna

4.1. Generation of harmonics

As mentioned in Section 3.2, for a low plasma density at the mouth of the box, $\bar{n}_i(x = 0) < 0.5 \times 10^{18}$ m^{-3}, the electric field penetrates into the layers in front of the box mouth, where it is shielded by the scrape-off layer plasma. Due to the large difference in the ion and electron masses (hence, in thermal velocities) and to the strongly non-linear plasma dynamics, there is a considerable asymmetry in the shielding of the antenna potential between the two half-periods of RF oscillations. The sinusoidal time variation of the potential at the central conductor is converted to a strongly non-sinusoidal signal at the box mouth (Fig. 10). The Fourier decomposition of this signal in a time series would contain harmonics. Indeed, the strong first harmonic signal with a significant parallel component of the field, pointing to

the electrostatic type of excitation, and with the amplitude of the same order as that of the fundamental one has been observed in front of the antenna box in experiments [24].

4.2. Generation of a stationary electric field

Along with harmonics, the RF field produces a stationary potential, which exhibits a 312 V hump (Fig. 11). This non-monotonic behavior can be understood as a consequence of the RF sheath rectification effect. At the position of the central conductor, the plasma is very rarefied, so the averaged potential is zero here. At the box mouth, the potential is shielded, and the amplitude of its oscillation is small. Consequently, the rectified potential is close to a floating of $\simeq 71.4$ V. So, the rectified potential has a profile with maximum at a position, where the plasma is dense enough to form a sheath and, hence, to rectify, yet not so dense as to have strongly shielded the potential oscillations. The ion density at the position, where the DC potential is maximum, is $\sim 10^{15}$ m^{-3}, and the greatest sputtering of ions from the walls due to the acceleration of plasma ions in the rectified potential can be expected beyond this radial position toward a denser plasma. The peak value of the rectified potential and the density at the position, where the DC potential has a maximum, depend only weakly on the density at $x = -d$ (boundary condition); the location of the maximum does, however, depend on this boundary density.

When the RF potential is not completely shielded within the antenna box, this causes the generation of a DC potential in front of the box. For the density $\bar{n}_i(x = -3) > 10^{19}$ m^{-3}, the magnitude of stationary potential at the box mouth deviates from the floating one by less than 11% of the latter. For a lower density $\bar{n}_i(x = -3) < 10^{18}$ m^{-3}, when the shielding is less effective, this deviation of the stationary potential is higher than 131%. In front of the box, this potential drops to the floating value within a distance of several millimeters, creating a strong radial DC electric field. The DC component of the potential can extend toroidally to a large distance much further than that for the AC component. In the region exterior to the box, but in its shadow (the region populated by the magnetic field lines, which intersect the box), the DC potential is driven by the RF field fringing from the box mouth and, hence, is sourced at the level of the mouth. It is thus plausible to anticipate a maximum in the DC potential at this radial level. Such a profile of the DC potential in the scrape-off layer has been observed in experiments with a shielded antenna [38].

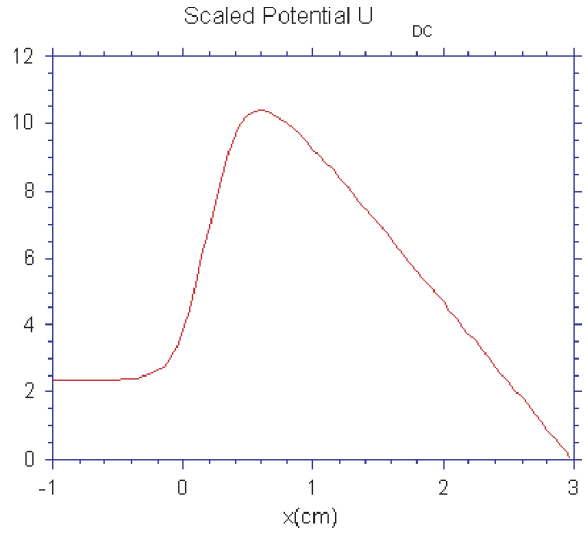

Fig. 11. DC component of $U = e\bar{\varphi}/T_e$ after 800 periods with a maximum inside the box and a descent to the floating potential outside it

4.3. Sheared poloidal flow

The DC component of the radial electric field can produce $\mathbf{E} \times \mathbf{B}$ stationary poloidal particle flows. Since the DC component of the potential field changes its sign inside the box, the particle flow due to $\mathbf{E} \times \mathbf{B}$ drift will have opposite directions on different sides of the potential maximum. Outside the box, the toroidally extended maximum of the DC potential just discussed should similarly drive a sheared flow. Though beyond the scope of the present poloidally invariant model, one might speculate as to a possible role such poloidal flow might play in the particle balance.

4.4. Density profile modification

Application of RF heating causes a drop of the density inside the box in the region of a strong electric field. Nonetheless, the particle flow along magnetic lines to the region in front of the antenna box (see Eqs. (17) and (18)) leads to an increase of the particle density in front of the box mouth in Fig. 12 (for comparison, a calculation done with no inflow of particles into the region in front of the box shows that the density drops everywhere in x). Though such an increase is in correspondence with certain experiments done with shielded antennas [38–40], one should accept the numerical result with some cau-

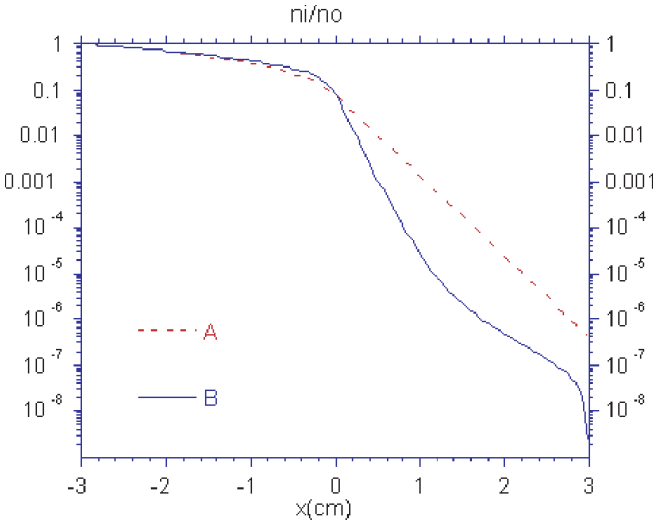

Fig. 12. Time-averaged ion density profile before *(curve A)*, and 800 periods after the RF excitation *(curve B)*

tion in view of the heuristic modeling embodied in the cited flow equations.

4.5. Power dissipation

The dissipation of the electric field energy in the antenna box occurs due to the acceleration of plasma particles along the magnetic field into the wall; the given drop of potential is located mainly in the sheath, such parasitic losses are dominated by the dissipation in the sheath. The power dissipation is taken as the average over the RF period of the integral of the product of the current density by the potential drop between the plasma and the grounded box wall over the antenna side walls:

$$P = 2hf \int_0^{1/f} dt \int_0^d dx\, e\varphi \left([nV_z]_i - [nV_z]_e \right). \qquad (21)$$

Here, h is the poloidal extension of the antenna box = 0.7 m, and the fluxes $[nV_z]_\alpha$ are given by Eqs. (12) and (13). The power dissipations are, respectively, 10.0, 11.6, 15.5, and 18.4 kW for $n_0 = 1$, 2, 10, and 20×10^{18} m^{-3}. A higher plasma density at the mouth of the box favors the current flow to the walls insofar as it increases charge carrier density. At the same time, it gives a better shielding of the potential inside the box. The variation of power dissipation with the density at the box mouth is a result of the competition between these effects: an increase of the current and a decrease of the potential. From the above figures, one indeed sees the non-linear dependence of the order-of-magnitude increase in the density causing a mere doubling of the power dissipation in the box. Without RF, as can be expected, the dissipated power is negligible (to within a precision of 10 W or less).

4.6. Current rectification

The RF field brings change in the net current that flows to the walls of the antenna box. This current is composed of two contributions. The first comes from the current, which flows into the box mouth and arrives at the walls from their inner sides; the second represents the current that impinges on the exterior of the box walls from the scrape-off layer.

In Table, we give various total current components flowing to the inner box walls of a poloidal extent of 0.7 m. These are the net current $J_{\rm RF}$ (with RF excitation), ion component $J^i_{\rm RF}$, and electron component $J^e_{\rm RF}$. Without RF, the electron current $J^e_{\rm st}$ that comes from the antenna box mouth cancels the ion current $J^i_{\rm st}$, giving no total current $J_{\rm st}$. There is also no z-wise flow of charged particles in front of the antenna box in this case. The RF excitation causes a growth of the potential in front of the box mouth (see Figs. 10 and 11), which attracts electrons to the region in front of the box and in a less degree repels ions. The electron current into the box mouth, $J^e_{\rm RF}$, is now not balanced by the ion current $J^i_{\rm RF}$, giving a net negative current to the box wall. From comparison of the ion $J^i_{\rm RF}$ and electron $J^e_{\rm RF}$ currents at various densities, it can be seen that the absolute value of the current of either species is larger, if the plasma density at the box mouth is higher. But their sum, which corresponds to the net current, is a non-monotonic function of the density. Thus, at $n_0 = 10^{19}$ m^{-3}, the total current $J_{\rm RF} = -38.3$ A gets its local maximum.

In experiments with FS, the box of an active antenna was found to draw an electron current of the order of 100 A during the RF heating, while the ion current was found to flow to the box of a second passive antenna [24–26]. Though the result without FS given in Table falls below this range measured with FS, it must be kept in mind that Table includes only that part of

T a b l e. Different current components (in A) flowing into the box mouth and, hence, to the walls from its interior. The components are given under RF excitation for three indicated densities n_0 at the radial position $x = -3$ cm

n_0	10^{18} m^{-3}	2×10^{18} m^{-3}	2×10^{19} m^{-3}
$J^e_{\rm RF}$	–21.9	–36.4	–106.7
$J^i_{\rm RF}$	1.5	4.2	70.6
$J_{\rm RF}$	–20.4	–32.2	–36.1

the current, which flows into the box mouth, by coming to the box walls from their inner sides. As already mentioned, another contribution can be given by the electron current that flows to the outer side of the antenna box walls from its shadow region. The reason for this is as follows. As shown in the previous sections, there is a potential oscillation just in front of the box of the active antenna. This alternating potential can penetrate radially into the shadow region of the antenna box, by causing a varying potential difference between the plasma in the box shadow and the grounded walls of the box. This potential is mostly above the floating value, but it oscillates below this value (see Fig. 10), by allowing the electron current to flow to active antenna's outer box walls in proportion to the high electron thermal velocity. The potential oscillation driven at the active antenna is damped toroidally, but the DC component of the potential penetrates toroidally to a much further distance than the fundamental and higher harmonics. It can easily reach the box of the passive antenna. The value of DC potential averaged over the RF period is above the floating value (see Fig. 11), by implying a net positive current to the wall of the passive antenna. Insofar as the total net current to the boxes of active and passive antennas should be zero, the net negative current must flow to the box of an active antenna to balance the net positive current flowing to the walls of a passive antenna. We mention the analogous considerations applied to the case of a different antenna geometry in [41]. Taking the DC potential at the box mouth ($x = 0$) to be as that in Fig. 11 and to persist over the outer box walls over a region Δx of the order of one or two centimeters, one finds the ion current density flowing to the passive antenna wall to be of the order of the Bohm value over Δx, with the total current over the 0.7 m poloidal box length being of the order of hundreds of Amperes. This corresponds to what was observed in experiments albeit done with FS. A more detailed calculation of this value falls outside the mathematical framework of our numerical model. Thus, the current rectification effect can be explained, at least qualitatively, on the basis of the foregoing considerations. The part of this current that comes into the box is directly calculated. An additional current component flowing to the outer side of the box wall can be explained from the penetration of the potential in front of the antenna box, also calculated in the model, with additional consideration of a spatial variation of this potential, radially and toroidally, in the shadow of the antenna box.

5. Discussion

The main elements of the dynamics of the plasma in an antenna box are quite general, comprising a balance of transverse and parallel particle transports coupled with shielding an external potential applied to the antenna central conductor. Should the particular transport process be changed, this will quantitatively influence the results, but will not qualitatively change the layered structure, which is formed in the antenna box during the RF excitation. Calculations have been made to check the sensitivity of results to the driving potential and plasma parameters, as well as to the certain assumptions of the model. Here, we briefly discuss to what extent a modification of the results can be expected.

When the frequency of the driven potential is low, $f \sim c_S/L$, the oscillation amplitudes of the two species are rather similar. At a high frequency, the shielding is due to more mobile electrons, with a variation of the ion density on the RF time scale becoming small. In this respect, the ion behavior resembles the high-frequency regime in a RF sheath [6, 7, 35], where ions move in the averaged potential and do not react to rapid oscillations.

With increase in the amplitude of the driving potential, the vacuum region becomes wider, and the charged layer is shifted to the box mouth. If the plasma density at the box mouth is not sufficient, a temporal variation of the potential extends to the layers in front of the box. The efficiency of the plasma shielding depends not only on the density, but also on the particle thermal velocity, especially that of ions. For higher velocities, the charged layer is thinner; in the opposite case, a lower degree of charge separation requires a thicker layer in order to accumulate the same charge during one half-period.

The effect of the poloidal component of the inductive field, E_y, has been considered in the extended model [22, 23]. It was found that E_y slightly varies in the radial direction, so there was only a minor effect on the density and potential profiles. This agrees with the assumptions of the present model (cf. Eqs. (7) and (20)) in view of the enormous effect of the potential field itself.

6. Conclusions

A model of self-consistent plasma dynamics in an antenna box with driven RF potential is proposed. The description of the transverse particle motion in a highly turbulent state typical of tokamak edge plasmas is reduced to a diffusion-type equation on the time scale of a RF variation. For the parallel motion, the standard probe theory has been generalized to the case of non-

quasineutral plasma. The non-linear equations of the model are treated numerically. Evolution of the particle density and potential radial profiles from a quiescent initial state through to an asymptotic oscillatory state with applied RF voltage, as well as their variation during a single RF period, haves been studied. Over the transient interval connecting the two limit states, the plasma density in a vicinity of the central conductor drops, and a layered structure is formed, a sublayer of this structure playing the role of a Faraday shield. The structure consists of: *(i)* – vacuum region near the antenna central conductor, *(ii)* – intermediate region of a non-quasineutral plasma with oscillating charge, and *(iii)* – quasineutral region, where the antenna potential has been shielded. The antenna potential is essentially shielded by the charged layer *(ii)*, this layer and the central conductor constituting the two "plates" of a capacitor.

The electric field power dissipation in the sheath at the antenna box walls has been calculated for self-consistent density and potential profiles; it is found to be small (of the order of 10–20 kW) in comparison with the radiated power (of the order of 1 MW). The rectified potential inside the box has a maximum ~ 300 V, with the corresponding ion density at this radial position $\sim 10^{15}$ m^{-3}, a possible cause of the sputtering of ions from the walls of the antenna box. However, the walls at this position are composed of carbon, being in fact portions of the antenna side limiters. Hence, the plasma contamination from the sputtering is not so critical as that in the case of a Faraday shield subjected to the RF sheath effect at its metallic surfaces. These findings support the idea that the ICRF antennas can operate without a Faraday shield.

The model points to the sole presence of a RF potential electric field to be sufficient for the generation of a number of phenomena observed in scrape-off layer plasmas, including the plasma density profile modification, current rectification, as well as harmonic and stationary field components. The last one plausibly drives a sheared $\mathbf{E} \times \mathbf{B}$ poloidal flow.

The author is grateful to members of the Laboratory of Plasma Physics ERM-KMS in Brussels for valuable discussions on particular problems of tokamak plasma.

1. M.A. Rothman, R.M. Sinclair, I.G. Brown, and J.C. Hosea, Phys. Fluids **12**, 2211 (1969).
2. V.P. Bhatnagar, G. Bosia, M. Bures *et al.*, in *Proc. of Joint Varenna-Grenoble Int. Symp.* (CEC, Brussels, 1978), Vol. 1, p. 133.
3. J. Jacquinot and T.F.R. Equipe, in *Proc. Internat. Conf. on Plasma Physics* (Fusion Res. Assoc. of Japan, Nagoya, 1980), Vol. 2, p. 226.
4. D. Faulconer, J. Appl. Phys. **54**, 3810 (1954).
5. F.W. Perkins, Nucl. Fusion **29**, 583 (1989).
6. R. Chodura and J. Neuhauser, in *Abstracts of the 16-th Eur. Conf. on Controlled Fusion and Plasma Physics* (Venice, 1989), Vol. 13B, Part III, p. 1089.
7. J.R. Myra, D.A. D'Ippolito, and M.J. Gerver, Nucl. Fusion **30**, 845 (1990).
8. E. Faudot, L. Colas, and S. Heuraux, Phys. Plasmas **13**, 042512 (2006).
9. R. Van Nieuwenhove, R. Koch, and G. Van Oost, LPP-ERM/KMS Brussels Laboratory Report **93**, (1990).
10. R. Van Nieuwenhove, R. Koch, and G. Van Oost *et al.*, Nucl. Fusion **31**, 1770 (1991).
11. R. Van Nieuwenhove, R. Koch, G. Van Oost *et al.*, Nucl. Fusion **32**, 1913 (1992).
12. J. Sorensenetal, Nucl. Fusion **33**, 915 (1993).
13. G.G. Borg and B. Joye, Nucl. Fusion **32**, 801 (1992).
14. S.J. Wukitch, B. Lipschultz, E. Marmar *et al.*, J. Nucl. Materials **363-–365**, 491 (2007)
15. J.-M. Noterdaeme *et al.*, in *Proceed. of the 16th Inter. Conf. on Fusion Energy* (IAEA (Vienna), Montreal, 1997), p. 335.
16. M. Bures *et al*, Nucl. Fusion **30**, 251 (1990).
17. M. Bures *et al.*, Nucl. Fusion **32**, 1139 (1992).
18. D.W. Swain, R.I. Pinsker, F.W. Baity *et al.*, Nucl. Fusion **37**, 211 (1997).
19. V.I. Zasenko, D.W. Faulconer, and R. Koch, in *Abstracts of the 24th European Conf. on Controlled Fusion and Plasma Physics, Berchtesgaden* (1997), **21A**, Part I, p. 449.
20. V.I. Zasenko, D.W. Faulconer, and R. Koch, in *Proceed. of the 7th European Fusion Theory Conference, Juelich* **1**, (1997) p. 295.
21. V.I. Zasenko, D.W. Faulconer, and R. Koch, LPP-ERM/KMS Brussels Laboratory Report **111** (1997).
22. V.I. Zasenko, in *Abstracts of the 25th European Conf. Controlled Fusion and Plasma Physics, Prague*, **22C** (1998), p. 1368.
23. V.I. Zasenko, Problems of Atomic Sci. and Techn. Ser: Plasma Physics **1(1)**, **2(2)**, 145 (1999).
24. R. Van Nieuwenhove and G. Van Oost, J. Nucl. Materials **162-164**, 288 (1989).
25. G. Van Oost, R. Van Nieuwenhove, R. Koch, *et al.*, Fusion Eng. Des. **12**, 149 (1990).
26. R. Van Nieuwenhove and G. Van Oost, Plasma Phys. Contr. Fusion **34**, 525 (1992).

27. D. Bohm, in: *Characteristics of Electrical Discharges in Magnetic Fields*, edited by A. Guthrie and R.K. Wakerling (McGraw-Hill, New York, 1949), p. 77.

28. P.C. Stangeby, J. Phys. D: Appl. Phys. **15**, 1007 (1982).

29. F.F. Chen, in *Plasma Diagnostic Techniques*, edited by R.H. Huddlestone and S.L. Leonard, (Academic Press, New York, 1965) p. 113.

30. P.C. Stangeby, in *Plasma Diagnostics*, edited by O. Auciello and D.L. Flamm (Academic Press, New York, 1989), Vol. 2, p. 157.

31. I.H. Hutchinson, *Principles of Plasma Diagnostics* (Cambridge Univ. Press, Cambridge, 1987).

32. A.T. Mense and G.A. Emmert, Nucl. Fusion **19**, 361 (1979).

33. B. LaBombard, R.W. Conn, and G. Tynan, Plasma Phys. Contr. Fusion **32**, 483 (1990).

34. J.-L. Lachambre *et al.*, Nucl. Fusion **34**, 1431 (1994).

35. M.A. Lieberman, IEEE Trans. Plasma Sci. **16**, 638 (1988).

36. R. Van Nieuwenhove, R. Koch, and G. Van Oost, in *Abstracts of the 21st Eur. Conf. Controlled Fusion and Plasma Physics, Montpellier* **18B**, (1994), Part II, p. 976.

37. H.S. Butler and G.S. Kino, Phys. Fluids **6**, 1346 (1963).

38. J.H. Harris *et al.*, in *Abstracts of the 21st Eur. Conf. Controlled Fusion and Plasma Physics, Montpellier* **18B**, (1994), Part II, p. 898.

39. D.A. D'Ippolito *et al.*, in *Proceed. of the 11th Topical Conf. on RF Power in Plasmas, Palm Springs* **355**, (1995) p. 467.

40. G.R. Hanson *et al.*, in *Proceed. of the 11th Topical Conf. on RF Power in Plasmas, Palm Springs* **355**, (1995) p. 463.

41. R. Majeski *et al.*, in *Proceed. of the AIP Conf. on Radio Freq. Power in Plasma, Charleston* (1991), **244**, p. 322.

Received 19.09.12

УТВОРЕННЯ ЗАРЯДЖЕНОГО ШАРУ В ОБМЕЖЕНІЙ НЕОДНОРІДНІЙ ЗАМАГНІЧЕНІЙ ПЛАЗМІ У ВЧ ПОЛІ

В.І.Засенко

Р е з ю м е

Запропоновано модель динаміки плазми у патрубку радіочастотної антени без фарадеєвого екрана, що застосовується для нагрівання плазми в токамаках. Передбачено утворення макроскопічного шару осцилюючого заряду, що виконує роль екрана. Обговорюється зв'язок з явищами, що спостерігались у периферійній плазмі токамаків.